Available online at www.sciencedirect.com
SCIENCE DIRECT®
Journal of Magnetic Resonance 166 (2004) 215–227
JMR Journal of Magnetic Resonance
www.elsevier.com/locate/jmr

Effects of residual single-quantum coherences in intermolecular multiple-quantum coherence studies

Geoffrey D. Charles-Edwards,[a] Geoffrey S. Payne,[a,*] Martin O. Leach,[a] and Angelo Bifone[a,b]

[a] *Cancer Research UK Clinical Magnetic Resonance Research Group, The Institute of Cancer Research and The Royal Marsden NHS Trust, Sutton, Surrey SM2 5PT, UK*
[b] *GlaxoSmithKline Research Centre, Verona 37128, Italy*

Received 9 July 2003; revised 20 October 2003

Abstract

Intermolecular multiple-quantum coherences (iMQCs) have been reported to offer a sensitivity to sample structure at a specific user-defined length scale down to the order of 10 μm. When assessing this novel contrast mechanism in controlled phantom experiments, we have observed three different mechanisms whereby residual single-quantum coherences (SQCs) arising from intense high spatial frequencies, stimulated echoes and strong spatially encoding gradients can produce significant changes in signal contrast at particular length scales. These changes which only appear when components arising from SQCs and iMQCs are both present in the detected signal, are similar to changes previously attributed to iMQCs alone. We demonstrate each mechanism by which these residual SQCs arise and describe methods for their suppression.

Keywords: Intermolecular multiple-quantum coherences; Signal contrast; Single-quantum coherences; Distant dipolar field; Dipolar correlation distance

1. Introduction

Intermolecular multiple-quantum coherences (iMQCs) have generated much interest and controversy over recent years. Perhaps the most important potential clinical application of iMQCs arises from their reported sensitivity to sample structure at spatial dimensions around a specific user-defined distance, known as the correlation distance, down to the order of 10 μm [1]. This specific sensitivity may offer the possibility of assessing sample structure in vivo on a length scale far below the typical MRI pixel size. Indeed, the potential of iMQCs has already been investigated in a number of human in vivo experiments, including fMRI [2,3], oncological studies [4], and the examination of trabecular bone for the study of osteoporosis [5]. Applications to the study of porous micro-structured materials have also been envisaged [6].

It is important to demonstrate that a novel technique can offer useful additional information if it is to be developed as a new diagnostic tool in MRI, and validation and characterization in controlled experimental conditions are an essential part of this work. To date there have been a number of reported phantom studies investigating the novel sensitivity of iMQCs to sample structure, using unlocalized measurements [7–10] and imaging experiments [11–13].

In spatially resolved studies of a simple structured phantom consisting of a water-filled NMR tube oriented parallel to the direction of the magnetic field, Bowtell and co-workers found decreasing signal intensity in a region of pixels located adjacent to the tube wall. The spatial extent of signal loss in this region varied with the selected length scale, and was in good agreement with theoretical predictions [11]. Warren and co-workers have examined more complex structures consisting of packed plastic straws and coffee stirrers in water. In imaging experiments with a coffee stirrer phantom, substantial changes in the image contrast were observed

* Corresponding author.
E-mail address: geoffrey.payne@icr.ac.uk (G.S. Payne).

1090-7807/$ - see front matter © 2003 Elsevier Inc. All rights reserved.
doi:10.1016/j.jmr.2003.10.017

when the correlation distance was made comparable to the size of the gaps between the stirrers [12]. However, higher resolution images appeared to show more modest contrast changes arising from pixels adjacent to the water-wall boundary [13].

In both of these imaging studies the effects of susceptibility mismatches were minimized by orienting the tubes parallel to the direction of the magnetic field, thereby focusing the investigation on the sensitivity of iMQCs to variations in magnetization density alone. Arguably, the suggestion that iMQCs should be sensitive to sub-pixel variations in the local magnetic field on a specific length scale is of more interest, since it is this property that would be applicable to fMRI, oncological, and other in vivo studies, where susceptibility mismatches, e.g., arising between blood and the surrounding tissue, give rise to perturbations in the magnetic field on a length scale determined by the structure, e.g., the size of the blood vessel. However, to date there have been relatively few reported phantom studies investigating the sensitivity of this technique specifically to local magnetic field perturbations.

Perhaps the most promising evidence of a sensitivity to susceptibility mismatches on a particular length scale has been reported by Maraviglia and co-workers [9,10]. When the magnitude of the unlocalized signal arising from intermolecular double-quantum coherences (iDQCs) in the Multiple Spin Echoes experiment was plotted as a function of correlation distance for a sample of closely packed glass beads (diameter = 1 mm) in water, they observed narrow signal dips at specific correlation distances, which appeared to coincide with characteristic length scales of the sample structure [9,10]. They proposed that these dips arose from the specific sensitivity to regular spatial variations in the local magnetic field resulting from the susceptibility mismatch between the glass beads and the surrounding water. Analogous narrow dips have been observed by the same authors in trabecular bone samples, and have been proposed as a means of assessing trabecular structure in healthy bone and in bone affected by osteoporosis [9]. Warren and co-workers [14] have also investigated trabecular bone specimens, and observed a single, much broader dip whose depth depended strongly on the relative orientation of the sample with respect to the direction of the magnetic field.

However, not all experimental observations have produced positive evidence for a specific sensitivity. For example, signal dips at specific correlation distances were not found in previous work with glass beads (diameters = 100, 200, and 400 μm) in water by Bowtell and co-worker [7], who observed only changes in the overall relationship between the signal magnitude and the selected correlation distance. More recently, Bowtell and co-workers [15] have simulated fMRI experiments by studying polystyrene beads suspended in a paramagnetic solution, creating susceptibility mismatches similar to those arising from capillary vessels in vivo. They found that the iDQC transverse relaxation rate was not sensitive to the selected correlation distance, for the range of length scales investigated [15,16]. Three-dimensional numerical studies of the iDQC-CRAZED signal in inhomogeneous solutions have also shown no significant dependence on the selected correlation distance, implying that the novel contrast cannot be tuned to susceptibility changes arising from blood vessels of a particular size [17].

In order to validate the novel contrast mechanism afforded by iMQCs, and to investigate its origin, we have performed experiments in structured phantoms closely resembling those reported in the literature. We found that a mixture of components arising from iDQCs and residual SQCs produces significant changes in the detected signal at certain correlation distances. These signal changes are similar to previously reported observations which have been ascribed to the novel properties of iMQCs alone. However, when the residual SQC component is suppressed, these signal changes are no longer observed. Thus, residual SQCs are a potential confounder in iMQC studies, and might explain some of the discrepancies reported in the literature. Three separate mechanisms giving rise to residual SQCs are investigated and demonstrated here from experimental work at 1.5 and 7 T, together with a description of methods for their suppression.

2. Theory

The dipolar interaction between nuclear spins is proportional to the second-order Legendre polynomial, $\mathscr{P}_2(\cos\theta) = (3\cos^2\theta - 1)/2$, where θ is the angle between the inter-spin vector and the direction of the magnetic field. In liquids the dipolar interaction between closely spaced nuclear spins essentially samples all values of θ via molecular diffusion during the time scale of an NMR experiment, and consequently averages to zero. For more distant nuclear spins, diffusion is no longer effective at cancelling out the dipolar interaction. These long-range dipolar interactions are nevertheless averaged to zero for a magnetically isotropic sample, as is the case for a spherical sample geometry. However, the application of a magnetic field gradient acts to destroy this isotropy and the restored distant dipolar interactions form a distant dipolar field (DDF). This additional magnetic field makes the Bloch equation nonlinear, and imposes a cosinusoidal variation in the precessional frequency [18].

In the multiple spin echoes (MSE) sequence, as shown in Fig. 1A, two RF pulses, with nutation angles of 90° and β, respectively, and a pulse interval τ, are applied to a sample in the presence of a continuous magnetic field

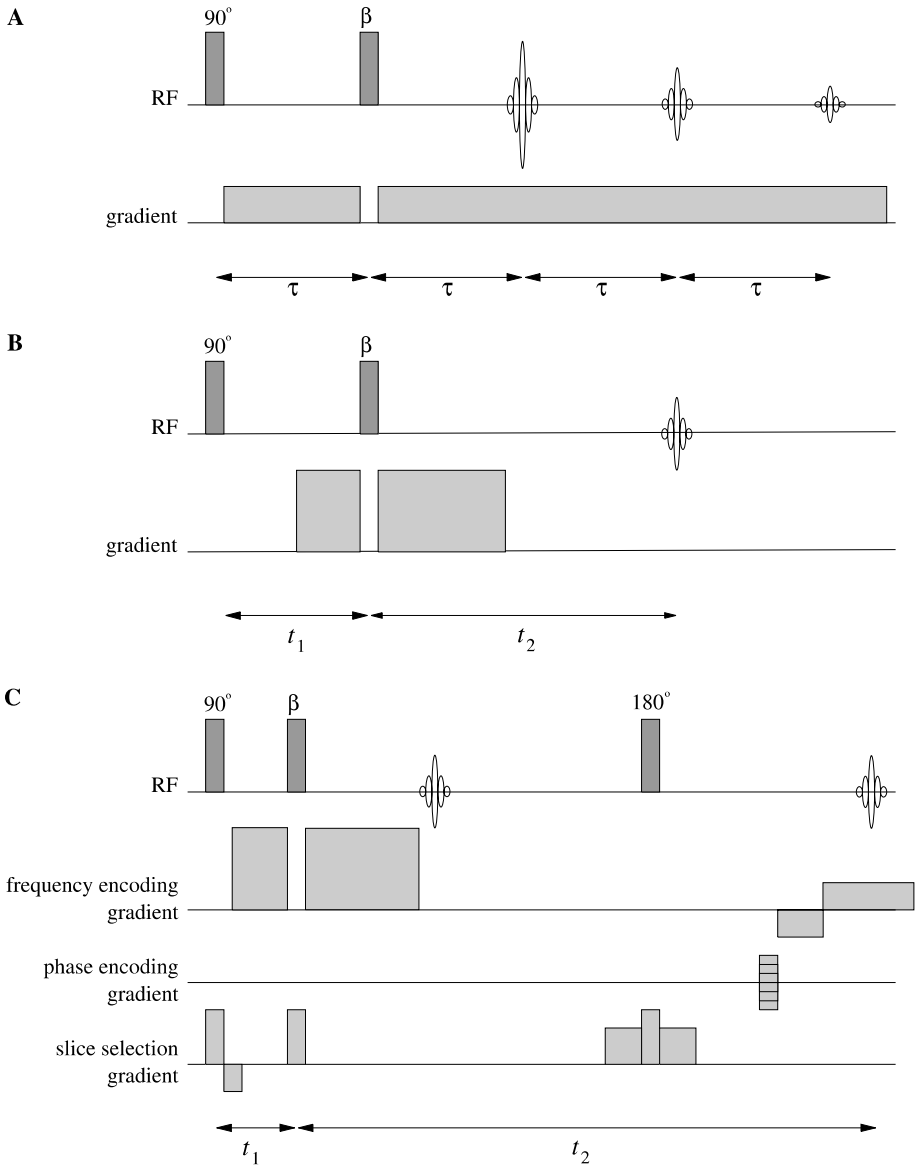

Fig. 1. (A) The multiple spin echoes (MSE) sequence. Following a series of two RF pulses, multiple spin echoes are observed when the magnetization evolves in the presence of a linear magnetic field gradient. When concentrating on the second echo one may consider the magnetic field gradient as a pair of gradient lobes around the second RF pulse, with a gradient area ratio of 1:2 (B). This is known as the iDQC-CRAZED sequence. The applied magnetic field gradient between the two RF pulses is also known as the correlation gradient. The iDQC-CRAZED imaging sequence in (C) was used in this work, based upon a conventional spin echo imaging acquisition. In this implementation an additional RF pulse was used to refocus the coherence echo, breaking the $t_2 = 2t_1$ dependence shown in sequence (B), and thereby allowing a larger detected signal magnitude to be obtained via an optimal short t_1 and long t_2.

gradient, of amplitude G. The solution to the modified Bloch equation, taking into account the additional DDF, can be expressed as series of harmonics. The conventional spin echo occurs at a time τ after the second RF pulse, with the harmonics refocused as a train of higher-order echoes occurring at $2\tau, 3\tau, \ldots$, when $\beta \neq 180°$ [18].

An alternative quantum mechanical explanation which can be applied to the MSE experiment has been developed by Warren and co-workers [1,19,20]. When the conventional high temperature approximation is omitted and higher-order terms are included in the expansion of the density matrix, the first RF pulse applied to the equilibrium magnetization creates iMQCs as well as SQCs. During the period between the two RF pulses, known as the evolution period, t_1, the applied magnetic field gradient spatially modulates the phase of the transverse magnetization. A proportion of this is converted into modulated longitudinal magnetization by the second RF pulse. Since the applied magnetic field gradient also makes the sample magnetization highly anisotropic, distant dipolar interactions do not average to zero. The second RF pulse converts a proportion of the iMQCs into multiple-spin anti-phase SQCs, which then

evolve via these long-range dipolar interactions into observable one-spin SQCs. Detectable signal originating from n-quantum coherences is refocused at a time nt_1 after the second RF pulse, e.g., the second echo in the MSE experiment arises from the existence of iDQCs during the evolution period. The magnitude of the signal arising from iDQCs is of the order of a few percent of the equilibrium magnetization at clinical magnetic field strengths, although this increases with higher magnetic fields. The classical and "Warren" treatments have been reported to give rise to equivalent predictions [21,22] and are considered here to be analogous.

The sensitivity to sample structure on a specific length scale arises since the dipolar field experienced at a particular location is predominantly dependent upon the surrounding magnetization found within one wavelength of the spatial modulation imposed by the magnetic field gradient, with a distribution around the so-called correlation distance, $d_c = \pi/\gamma G\tau$, where γ is the gyromagnetic ratio [1]. This selected length scale is therefore user-definable, since the correlation distance is determined by the strength and duration of the applied magnetic field gradient.

When concentrating on the second echo in the MSE experiment, it is often useful to consider the applied magnetic field gradient as a pair of gradient lobes around the second RF pulse, with a gradient area ratio of 1:2. This forms what is known as the iDQC-CRAZED sequence [1], as shown in Fig. 1B. The iDQC-CRAZED sequence has several advantages over the original MSE sequence including lower diffusion weighting and the freedom to apply independent spatially encoding gradients in conjunction with the signal acquisition, to produce an image arising from iDQCs.

From the theoretical description of iDQCs in unstructured samples and neglecting the effects of relaxation, diffusion, and resonance offset, the complex transverse magnetization, $M_+ \equiv M_x + iM_y$, at the time of the second echo is given by

$$M_+ = -iM_0\left[\left(\frac{1+\cos\beta}{2}\right)J_1\left(\frac{\Lambda_s t_2 \sin\beta}{\tau_d}\right) + \left(\frac{1-\cos\beta}{2}\right)J_3\left(\frac{\Lambda_s t_2 \sin\beta}{\tau_d}\right)\right], \quad (1)$$

where $J_n(x)$ is a Bessel function of order n, t_2 is the time after the second RF pulse, $\Lambda_s \equiv (1-3\cos^2\theta_s)/2$, θ_s is the angle between the direction of the applied magnetic field gradient and the direction of the magnetic field, and $\tau_d \equiv 1/\mu_0\gamma M_0$ is the so-called dipolar demagnetizing time [19,23,24]. For ^{1}H in pure water, 300 K, at 1.5 and 7 T, where τ_d is 630 and 135 ms, respectively [25], Eq. (1) predicts the maximum detected signal to occur when $t_2 \approx 1300$ and 300 ms, respectively. These maxima are difficult to reach in practice due to signal decay via transverse magnetization and diffusion. To minimize relaxation losses, most experimental phantom studies have been performed in water, where the transverse relaxation time is long. However, the associated lengthy longitudinal relaxation times require the use of long repetition times between excitations for effectively full relaxation to occur. Insufficiently long repetition times may give rise to potentially significant stimulated echo contributions in the detected signal.

3. Methods

Experiments were performed on a Siemens Vision 1.5 T MRI system and a Bruker Avance horizontal bore 7 T MRI system. The extremity volume RF coil (inner diameter = 20 cm) and a home-built saddle RF coil (length = 15 cm, inner diameter = 5 cm) were used on the Siemens MRI system and a birdcage volume RF coil (inner diameter = 6.5 cm) was used on the Bruker MRI system. Unlocalized iDQC-CRAZED sequences were implemented on both systems, and a MSE sequence was implemented on the 7 T system. An iDQC-CRAZED imaging sequence was also implemented on both systems. This was based upon a spin echo imaging sequence, using sinc RF pulses applied in conjunction with a slice selecting gradient, acquiring a single echo per excitation. Each of these sequences is shown in Fig. 1.

Three sets of experiments were performed. The first of these was designed to look at the role of phase cycling in the MSE sequence. This work was performed at 7 T closely matching previously reported experimental conditions [10]. A Perspex sphere (outer diameter = 5.5 cm) was filled with glass beads (diameter = 1 mm). This was periodically agitated during filling, to ensure the beads were closely packed, after which the inter-bead space was filled with tap water. A second Perspex sphere was filled with tap water, without glass beads. Non-selective rectangular RF pulses of 150 and 200 μs duration were calibrated to give nutation angles of 90° and 120°, respectively. A series of MSE acquisitions was performed over a range of correlation distances, by varying the evolution time, τ. Thirty-two signal averages were acquired at each evolution time. The correlation gradient was oriented along the x-axis, and applied with an amplitude of 19.8 mT/m. A repetition time, T_R, of 10 s was used. Acquisitions were performed with no phase cycling, a two-step phase cycle and a four-step phase cycle. The two-step phase cycling scheme ($\phi_1 = 0°, 180°$; $\phi_2 = 0°, 0°$; and $\phi_{rec} = 0°, 0°$) suppresses the contributions from odd-numbered quantum coherences in the evolution period, where ϕ_1 and ϕ_2 are the phase of the first and second RF pulses, respectively, and ϕ_{rec} is the receiver phase. Further suppression of $4n$-quantum coherences is achieved via a four-step phase cycle ($\phi_1 = 0°, 90°, 180°, 270°$; $\phi_2 = 0°, 0°$, $0°, 0°$; and $\phi_{rec} = 0°, 180°, 0°, 180°$), where $n = 0, 1, 2, 3, \ldots$ [21].

The second set of experiments examined the effect of additional contributions to the detected signal arising from stimulated echoes. This work was performed at both field strengths. At 1.5 T a collection of glass capillary tubes (inner diameter = 1.1 mm) was tightly packed into a plastic beaker (diameter = 6 cm) and filled with tap water, taking care to remove visible air bubbles. Another phantom was constructed in a similar manner using smaller tubes (inner diameter = 420 μm). Phantoms were placed at the centre of the extremity volume RF coil at the magnet isocentre. The capillary tubes were oriented perpendicular to the magnetic field, thereby generating a regular network of local magnetic field variations arising from the magnetic susceptibility mismatch between the water and the glass, as well as variations in the magnetization density. The correlation gradient was oriented parallel to the direction of the magnetic field to obtain the maximum signal arising from iDQCs. A series of unlocalized iDQC-CRAZED acquisitions was performed over a range of correlation distances, using the four-step phase cycling scheme described above. The correlation distance was varied by modifying the amplitude of the correlation gradient, keeping the timing of sequence events unchanged. Various repetition times between 2 and 15 s were investigated, giving rise to a larger or smaller stimulated echo contribution, respectively. The components of the detected signal arising from stimulated echoes and iDQCs were then acquired separately, using the modifications to a pair of iDQC-CRAZED sequences shown in Fig. 2. To detect only the signal arising from iDQCs, two iDQC-CRAZED sequences were executed in succession, with gradient area ratios of 1:2:2:4. The stimulated echo (coherence transfer pathway = +1,0,+1,−1) in this case is not refocused. To acquire only the signal arising from stimulated echoes, gradient area ratios of 1:2:2:3 were used. This arrangement refocuses the stimulated echo pathway but dephases the signal arising from iDQCs. Similar experiments were performed at 7 T with a water phantom closely packed with glass tubes (inner diameter = 1 mm). In this case the tubes were oriented parallel to the direction of the magnetic field, thereby minimizing the effects of the glass–water susceptibility mismatch, and giving rise to variations in magnetization density only.

The third set of experiments was based upon the iDQC-CRAZED imaging sequence at 1.5 T. A plastic beaker (diameter = 2.5 cm) containing closely packed

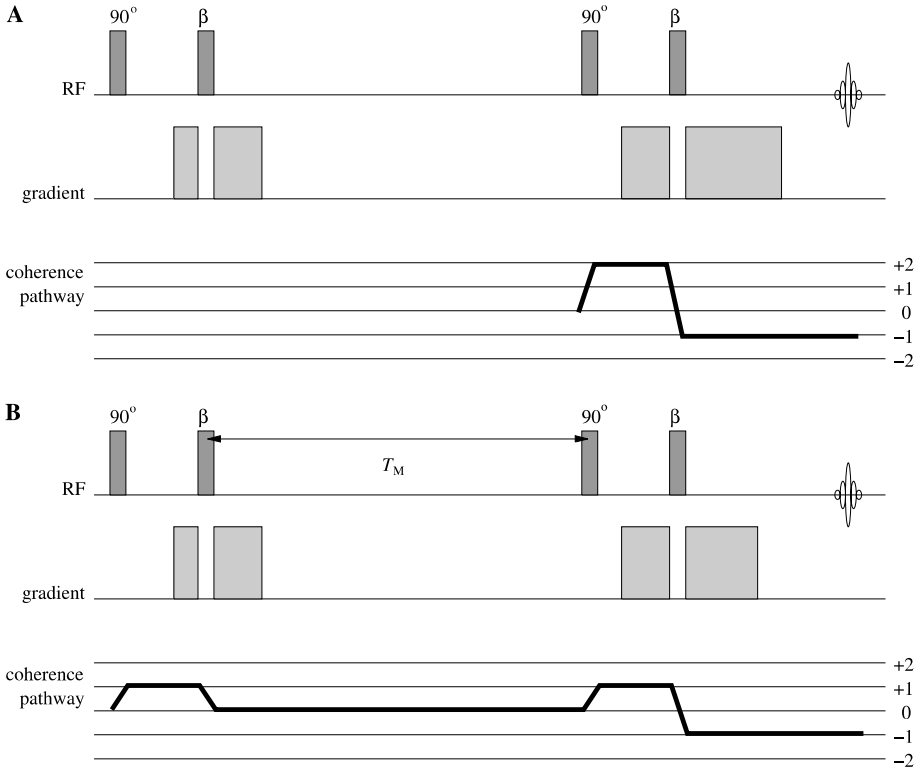

Fig. 2. Two pairs of iDQC-CRAZED sequences modified to refocus the signal component arising only from iDQCs (A) or the stimulated echo (B). The mixing time, T_M, is essentially equivalent to the repetition time when performing multiple iDQC-CRAZED acquisitions. The stimulated echo (coherence transfer pathway = +1, 0, +1, −1) is not refocused in (A) where the gradient area ratios are 1:2:2:4, whilst the iDQC pathway (+2,−1) is refocused. Conversely in (B) with gradient area ratios of 1:2:2:3, the iDQC pathway is dephased, and the stimulated echo pathway is refocused. When the correlation distance is calculated from the area of the first gradient lobe in sequence (B), the diffusion weighting for the stimulated echo arising from the applied gradients is similar to that found in multiple acquisitions of the basic iDQC-CRAZED sequence, shown in Fig. 1B.

glass capillary tubes (inner diameters = 1.1 mm) was filled with water, taking care to remove visible air bubbles. The phantom was then placed inside the 5 cm diameter saddle RF coil at the magnet isocentre. The capillary tubes were oriented perpendicular to the direction of the magnetic field to form a regular network of local magnetic field variations arising from the glass–water magnetic susceptibility mismatch, together with variations in the magnetization density. The correlation gradient was oriented parallel to the direction of the magnetic field to obtain the maximum signal arising from iDQCs. High resolution iDQC-CRAZED images were obtained over a range of correlation distances, adjusted by varying the amplitude of the correlation gradient.

4. Results and discussion

4.1. Unlocalized multiple spin echoes experiments: phase cycling

When the magnitude of the second echo in the MSE experiment is plotted as a function of the inter-pulse time, τ, for the phantom containing glass beads, a series of signal dips are observed when no phase cycling is used, as shown in Fig. 3A. These dips are not found when repeating the measurement without the beads, as demonstrated in Fig. 3B. This response appears to be consistent with previous observations [9,10], suggesting that the dips arise from the sample structure. The sampling resolution in both these cases was $\Delta\tau = 0.5$ ms.

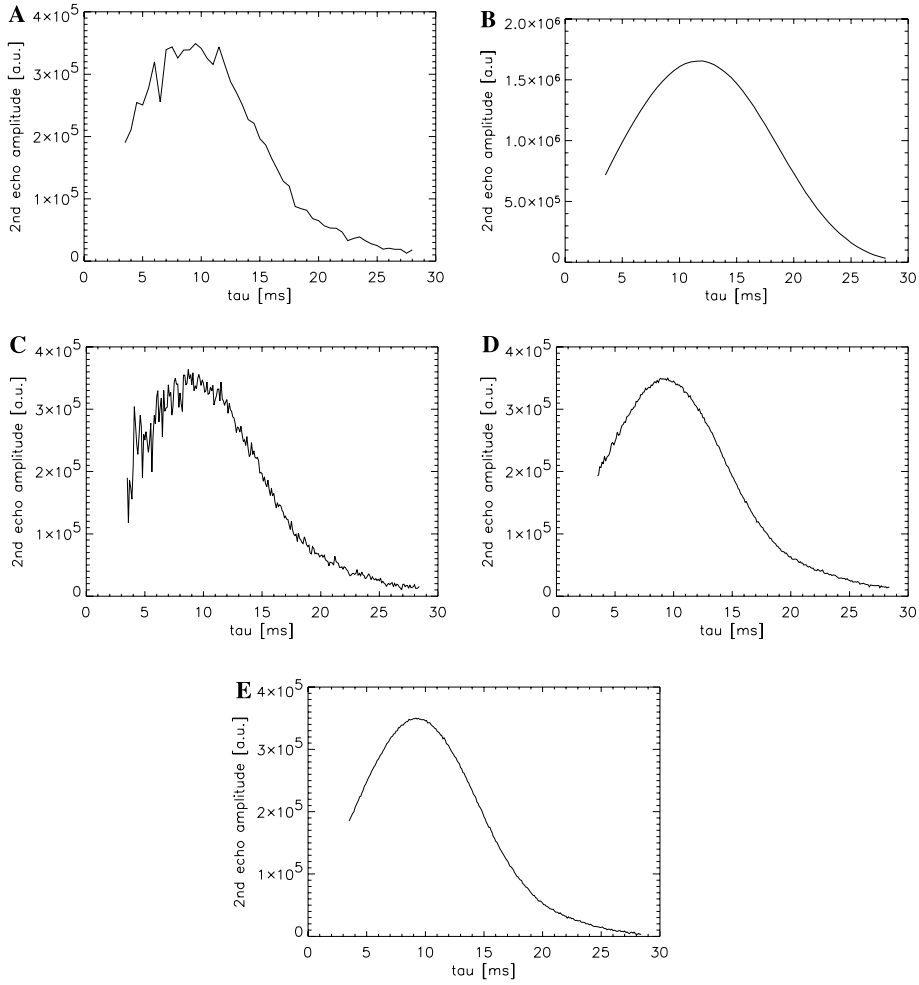

Fig. 3. The magnitude of the second echo from the MSE sequence at 7 T, as a function of evolution time, τ, for a phantom of closely packed glass beads surrounded by water. The first and second flip angles were 90° and 120°, respectively. The magnetic field gradient was oriented along the x-direction and was applied with an amplitude of 19.8 mT/m. The T_R was 10 s and the number of signal averages was 32. (A) The data acquired without phase cycling (sampling resolution $\Delta\tau = 0.5$ ms) suggesting a series of signal dips at particular values of τ. These dips are not observed when repeating the measurement for a bulb of water without beads (B), suggesting that these features arise from the sample structure. When a higher sampling resolution of $\Delta\tau = 0.1$ ms is used with the beads phantom, a more complex behaviour is revealed (C). When the experiment is repeated using the two-step phase cycling scheme to suppress odd-numbered coherences, a simpler signal response is observed (D). The four-step phase cycling scheme (E) offering additional suppression of $4n$-quantum coherences, where $n = 0, 1, 2, 3, \ldots$, smoothes the signal response further. The data in plots (D) and (E) were acquired with a sampling resolution of $\Delta\tau = 0.1$ ms.

When the sampling resolution was increased to $\Delta\tau = 0.1$ ms a more complex relationship between signal amplitude and the selected length scale was observed, as shown in Fig. 3C. When the experiment was repeated using the two-step phase cycling scheme ($\phi_1 = 0°, 180°$; $\phi_2 = 0°, 0°$; and $\phi_{rec} = 0°, 0°$) to suppress odd-numbered coherences, a simpler signal response was observed, as shown in Fig. 3D. The four-step phase cycling scheme ($\phi_1 = 0°, 90°, 180°, 270°$; $\phi_2 = 0°, 0°, 0°, 0°$; and $\phi_{rec} = 0°, 180°, 0°, 180°$), offering additional suppression of zero- and four-quantum coherences, smoothed the signal response further, as shown in Fig. 3E. The consistency of the data shown in Figs. 3D and E suggests that the lower number of signal averages when compared to similar previous experiments [9,10] did not significantly compromise the SNR in this case.

The origin of the observed dips when no phase cycling is employed is revealed when looking at the *k*-space data as a function of time. For a relatively unstructured sample, such as the phantom of water with no beads, the first and second echoes in the MSE experiment are clearly separated when no phase cycling is used, as demonstrated in Fig. 4A. Although the MSE sequence is unlocalized, the signal is detected in the presence of a magnetic field gradient, and consequently is frequency encoded. This is equivalent to acquiring the central line of *k*-space for an imaging sequence in the absence of phase encoding gradients, where high spatial frequencies are found on either side of the echo peak. When performing the same MSE experiment for the phantom packed with glass beads, the high spatial frequencies arising from the sample structure are observed after the main signal peak to extend into the second echo, as shown in Fig. 4B. Consequently the signal acquired at the second echo has components that arise from both iDQCs and SQCs.

Suppression of the first echo by approximately two orders of magnitude (not shown) was observed when the two-step phase cycle was employed. The high spatial frequency components of the first echo were similarly suppressed as shown in Fig. 4C. The four-step phase cycle, appears to improve this suppression slightly and has the additional advantage in this case of compensating for the DC offset, as demonstrated in Fig. 4D.

Previously, it was suggested [9] that the absence of signal dips in the original MSE experiments with structured samples [7] may have been due to insufficient sampling of different correlation distances. However, the very narrow linewidths of the signal dips observed by Maraviglia and co-workers, less than 10 μm in some cases, appear to have been adequately sampled in the earlier work [7]. Perhaps a more important difference between the two experiments is that the sequence used in the original work by Bowtell and co-workers employed an additional RF pulse midway through the evolution period to refocus the effects of magnetic field

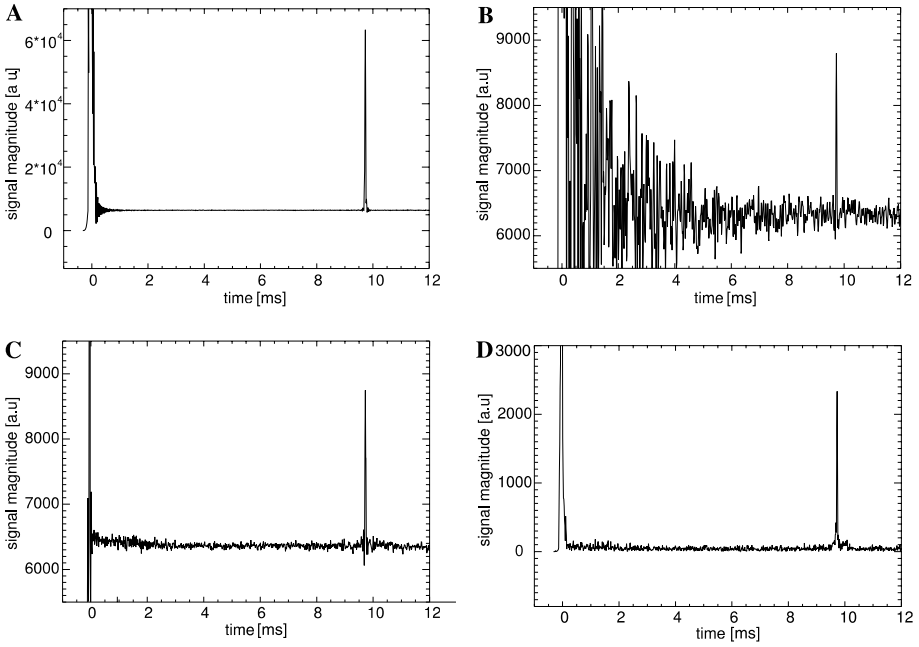

Fig. 4. The acquired signal magnitude from the MSE sequence at 7 T as a function of time. The gradient strength was 19.8 mT/m, with 32 signal averages and $T_R = 10$ s. The signal acquisition was started just prior to the first echo, and is plotted with the first echo occurring at 0 ms. The second echo occurs at 9.7 ms. The vertical axis is scaled to the magnitude of the second echo, and consequently the peak of the first echo is not shown. Plot (A) shows the results for a water phantom with no beads and no phase cycling. Plot (B) gives the results for the phantom packed with glass beads, showing the residual high spatial frequency components of the first echo that persist through the second echo. The first echo, together with its high spatial frequency components is suppressed when using the two-step phase cycle (C). The four-step phase cycle improves this suppression slightly, as shown in plot (D), and has the additional advantage of compensating for the DC offset.

inhomogeneities. If the signal dips observed by Maraviglia and co-workers were due to the sensitivity to local magnetic field perturbations arising from susceptibility mismatches, then these two experimental observations may be compatible. However, the data shown here offer an additional important reason for the disparity in observations, since phase cycling appears not to have been used in all previous work.

4.2. Unlocalized iDQC-CRAZED experiments: stimulated echoes

The detected signal magnitude from the unlocalized iDQC-CRAZED sequence for the phantom of glass tubes (inner diameter = 1.1 mm) in water, is displayed as a function of correlation distance in Fig. 5. A broad dip is observed with a minimum occurring at a correlation distance of 460 μm. This dip is similar to the broad dip observed by Warren and co-workers [14] in similar phantoms, and in trabecular bone. When the tubes were removed and replaced with water, this signal dip was not found. For the second phantom containing smaller tubes (inner diameter = 420 μm), a dip in the iDQC-CRAZED signal was again observed, this time with the minimum at the shorter correlation distance of 200 μm. These data are also shown in Fig. 5.

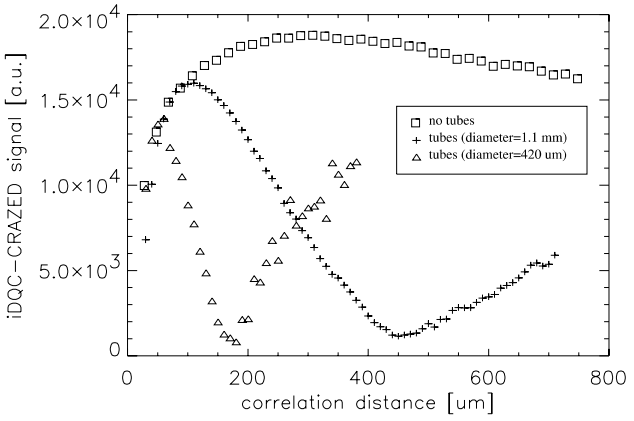

Fig. 5. The iDQC-CRAZED signal magnitude as a function of correlation distance for a plastic beaker filled with water, with and without an array of closely packed glass tubes of inner diameter 1.1 mm, and a second phantom containing smaller glass tubes of inner diameter 420 μm, again filled with water. The 420 μm diameter capillary tube data were acquired with a T_R of 5 s. Other data were acquired with a T_R of 6 s. All measurements were performed at 1.5 T employing the four-step phase cycling scheme described previously. The applied magnetic field gradient and the capillary tubes (when present) were oriented parallel and perpendicular to the direction of the magnetic field, respectively. The three datasets have been vertically scaled separately to fit onto one plot.

Again, these observations appear to be consistent with the hypothesis that the position of the dip reflects a characteristic length scale of the sample structure. However, the position of the dip was also observed to be sensitive to other sequence parameters such as the repetition time, and when the water was replaced with a 0.1 mM $MnCl_2$ + 90 mM NaCl solution to reduce the relaxation times towards those found in vivo, no dip was found. These data are shown in Fig. 6. Using unlocalized inversion recovery and spin echo sequences, the longitudinal and transverse relaxation times were measured for the tap water in the tubes phantom as 2668 ± 1 and 604 ± 5 ms, respectively, and for the doped solution as 652 ± 3 and 77.6 ± 0.3 ms, respectively.

The behaviour observed in Fig. 6 suggests a stimulated echo contribution to the detected signal. This hypothesis is confirmed by results from the modified paired iDQC-CRAZED sequences, shown in Fig. 7, where the the stimulated echo and iDQC components of the detected signal were separately isolated. The stimulated echo has a larger diffusion weighting than the signal component arising from iDQCs, since the interval between dephasing and rephasing gradient lobes is essentially equal to the repetition time. Consequently at short correlation distances, where the gradient amplitude is large, diffusion weighting is substantial and the stimulated echo component is heavily suppressed. However, the stimulated echo component may become larger than the component arising from iDQCs at long correlation distances, where the gradient amplitude, and hence diffusion losses, are smaller.

Neither the two-step or four-step phase cycles suppress the stimulated echo. Furthermore, when executing the four-step phase cycle in the order described above,

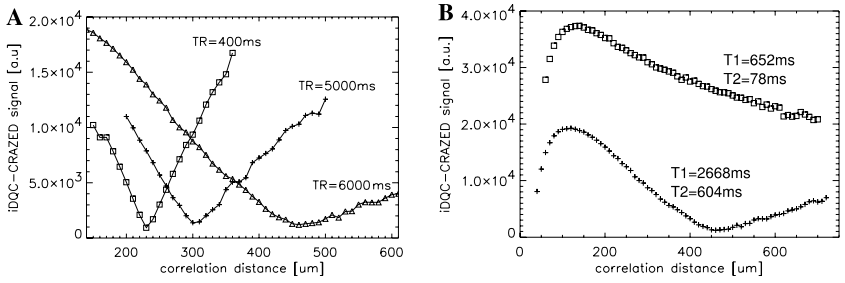

Fig. 6. The unlocalized iDQC-CRAZED signal as a function of correlation distance for a phantom of glass capillary tubes. Plot (A) shows the results obtained for the tubes in water at various repetition times. Plot (B) shows the results obtained with $T_R = 6$ s, for the tubes in water and in a solution of 0.1 mM $MnCl_2$ + 90 mM NaCl. Both experiments were performed at 1.5 T.

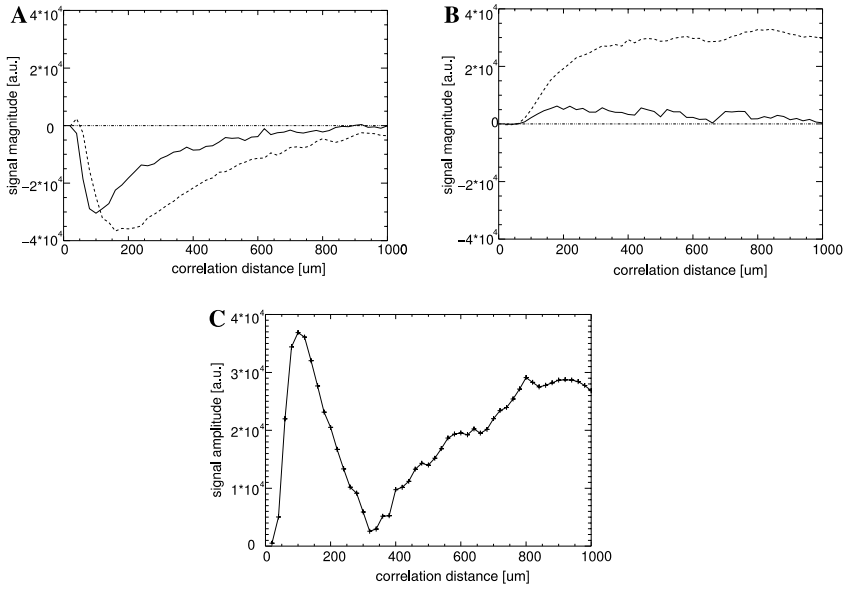

Fig. 7. Real (solid line) and imaginary (dashed line) signals arising from iDQCs (A) and stimulated echoes (B) in the iDQC-CRAZED sequence using the modified pair of iDQC-CRAZED sequence described previously (Fig. 2) with the four-step phase cycling scheme. These data were acquired at 7 T, with $T_R = 4$ s and one signal average, using the closely packed array of glass capillary tubes in water, with the tubes aligned parallel to the direction of the magnetic field. The correlation gradient was also aligned parallel to the direction of the magnetic field. Measurements are plotted as a function of the selected correlation distance. Plot (C) shows the magnitude of the complex summation of (A) and (B), revealing a signal dip at a particular correlation distance, which arises when the two components cancel.

the stimulated echo will be out of phase with the signal arising from iDQCs. In this case, at a particular intermediate correlation distance, the iDQC and stimulated echo components will be of equal magnitude and opposite phase, and will therefore cancel. When plotting the magnitude of the acquired iDQC-CRAZED signal against the selected correlation distance, this cancellation will appear as a signal dip. Similar results to those displayed in Fig. 7 were found at 1.5 T (data not shown). Since the signal arising from iDQCs is larger at 7 T, a shorter T_R than that used at 1.5 T was required to obtain a stimulated echo component with similar magnitude.

Nevertheless, the disappearance of the observed signal dip in Fig. 5 when the tubes are removed from the phantom suggests some sensitivity to sample structure. This arises predominantly from changes in the stimulated echo component rather than the component arising from iDQCs. The suppression of the stimulated echo without the presence of the tubes, as shown in Fig. 8B, may be related to bulk motion, which is reduced by the presence of the tubes. This hypothesis is supported by results shown in Fig. 8C from a similar phantom without tubes, where the bulk motion of water was inhibited by a gel matrix (6% polyacrylamide). Apparent diffusion coefficients of $1.17 \times 10^{-3} \pm 0.20 \times 10^{-3}$ and $1.07 \times 10^{-3} \pm 0.01 \times 10^{-3}$ mm^2/s were fitted as mono-exponentials to the water and gel data in Figs. 8B and C, respectively, for gradient b-values above 300 s/mm^2. Gradient b-values were calculated using the conventional Stejskal–Tanner expression [26], $b = \gamma^2 G^2 \delta^2 [\Delta - (\delta/3)]$, where δ is the duration of the first gradient pulse and Δ is the time separation between the dephasing and refocusing gradients, the first and last gradient pulses in Fig. 2B. The additional diffusion weighting arising from the third and fourth gradient pulses in this case is assumed to be negligible. This result confirmed that the gel matrix had little effect on the true diffusion. There was also little difference in the longitudinal relaxation times, measured as 2714 ± 5 and 2660 ± 7 ms for the water and gel, respectively.

Stimulated echoes are more significant in iMQC experiments than conventional SQC studies, since the signal arising from iMQCs is considerably smaller than the conventional MR signal, from which the stimulated echo originates. A calculation of the stimulated echo magnitude from a 90°–120°–90°–120° sequence in water ($T_1 = 2.7$ s, $T_2 = 1.5$ s, measured at 1.5 T), for a mixing time of 7 s, gives a magnitude of 3% of the equilibrium magnetization, similar in size to the signal arising from iDQCs. Although the contribution from stimulated echoes may be suppressed by going to very long repetition times, more elegant methods are available. After each signal acquisition Warren and co-workers spoil any remaining transverse and longitudinal magnetization by applying a gradient pulse followed by a 90° RF pulse and a second gradient pulse [13,27]. The gradients are oriented at the magic angle to avoid further DDF effects. Another technique to avoid refocusing stimulated echoes involves varying the direction of the correlation gradient slightly in consecutive excitations [25]. However, this may have negative implications when

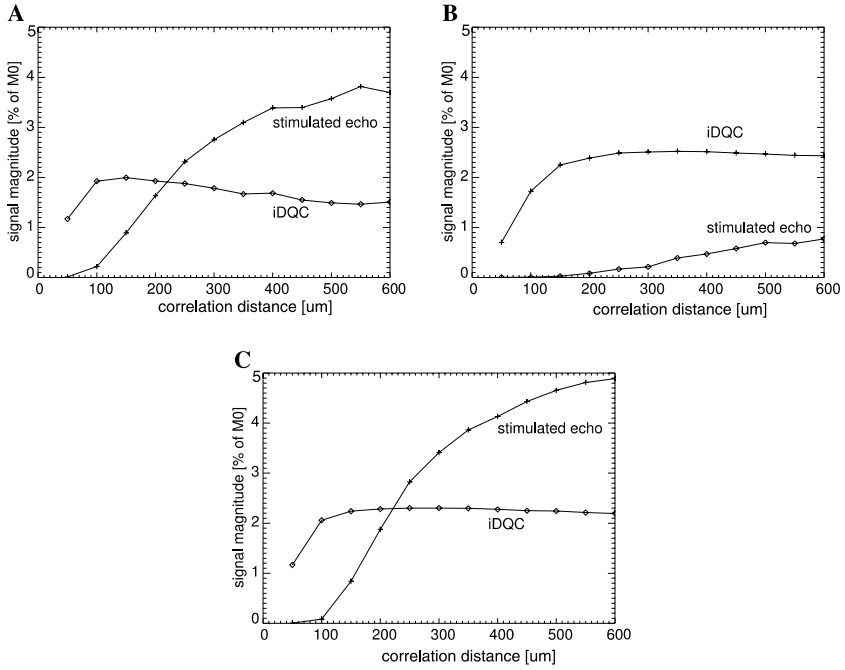

Fig. 8. Measured iDQC-CRAZED signal components arising from stimulated echoes and iDQCs, obtained using the modified sequences shown in Fig. 7. The data are plotted as a function of correlation distance for the phantom with (A) and without (B) glass tubes. Results for a similar phantom without tubes, but with bulk motion of the water inhibited by a gel matrix are shown in (C). These data were acquired at 1.5 T without phase cycling, with $T_R = 4$ s and number of signal averages = 1. The correlation gradient was oriented parallel to the direction of the magnetic field. The signal was referenced to that from the equilibrium magnetization, M_0, by performing a spin echo sequence (with a short echo time to minimize transverse relaxation).

acquiring signal from samples where the structure is highly anisotropic.

We have implemented an alternative gradient cycling based approach when performing the iDQC-CRAZED experiment over a range of correlation distances. In this case, rather than executing each step of the phase cycle in succession for a particular correlation distance, acquisitions are interleaved between different correlation distances. Consequently, the gradient areas are not balanced in adjacent sequences, and the stimulated echo pathway is not refocused. Using this approach we have suppressed the stimulated echo component from the iDQC-CRAZED acquisition, without the need for long repetition times. A comparison of results with and without gradient cycling is shown in Fig. 9. For the gradient cycled data, a very high sampling resolution was used to minimize the possibility of missing any narrow dips. With the stimulated echo contribution suppressed, the results give no indication of any signal dip over the range of correlation distances investigated.

A simple form of gradient cycling can be implemented into an iDQC-CRAZED imaging sequence, by ensuring that each successive excitation is followed by a different phase encoding, i.e., sequentially traversing k-space, rather than collecting the same line multiple times before incrementing the phase encoding gradient. This was used in the imaging acquisitions shown below.

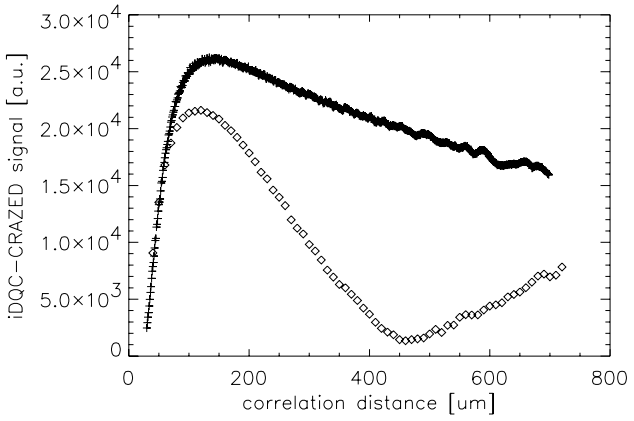

Fig. 9. The iDQC-CRAZED signal as a function of correlation distance for a sample of capillary tubes in water oriented perpendicular to the magnetic field, with (+) and without (◇) gradient cycling. These data were acquired at 1.5 T with $T_R = 6$ s and four signal averages using the four-step phase cycle. The correlation gradient was oriented parallel to the direction of the magnetic field.

4.3. iDQC-CRAZED imaging

With no phase cycling, iDQC-CRAZED images acquired with correlation distances of 120 and 460 μm, corresponding to the maximum and minimum points found in the initial unlocalized measurements, shown previously in Fig. 5, revealed a significant change in

image contrast. The iDQC-CRAZED image acquired at a correlation distance of 120 μm resembled a conventional MR image (data not shown), while at the longer correlation distance a "fuzzy" image was observed. This result appeared to be similar to previously reported observations [12]. However, upon inspection of the *k*-space data, it was discovered that this change in image contrast was due to interference from the conventional SQC echo. Although the initial 1:2 gradient ratio in the iDQC-CRAZED sequence dephases non-DQCs, the strength of the applied spatially encoding gradient may be such that at some point after the centre of *k*-space the effective gradient ratio is reduced to 1:1, at which point the SQC echo occurs. This problem was first highlighted by Bowtell and co-workers [11], and has recently been demonstrated by Warren and co-workers [13].

Figs. 10A and B show the raw and image data, respectively, for a "fuzzy" image, where the SQC echo can be seen at the right edge of the *k*-space data. If the imaging sequence is repeated using the two-step phase cycling scheme described above, this SQC echo is greatly suppressed, and a sharper, more conventional image contrast is regained following the FFT, as shown in Figs. 10C and D. The refocusing of other coherence pathways is more clearly observed when extending the duration of the signal acquisition in conjunction with the applied spatially encoding gradient, as shown in Fig. 10E. These observations demonstrate that the SQC

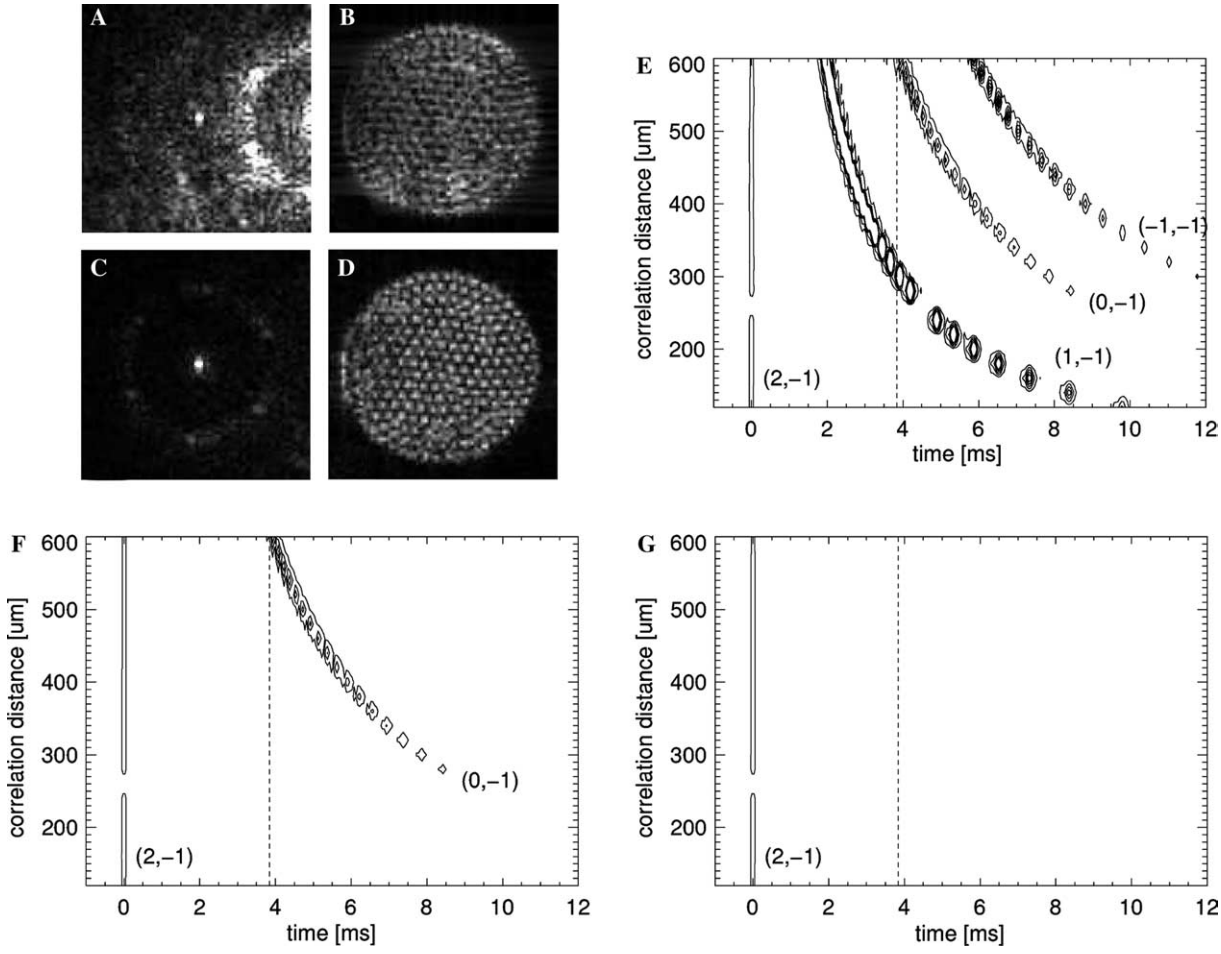

Fig. 10. (A) The *k*-space data for the iDQC-CRAZED image through a collection of capillary tubes in water, showing a second echo towards the right-hand side of the raw data. The interference from the second echo gives rise to a "fuzzy" image contrast (B) after performing the FFT. When acquiring the image data using a two-step phase cycle, this interference is significantly reduced (C) and a more regular image contrast is observed (D). The contour plot (E) shows the detected signal with time, acquired in the presence of a frequency encoding gradient with no phase cycling. The refocusing of the iDQC pathway (+2, −1) occurs at time = 0. However, the continuing application of the frequency encoding gradient acts to refocus other coherence pathways. Echoes arising from these other coherence pathways start to appear during the imaging ADC window, the extent of which is indicated here by the dashed line, when the correlation distance exceeds approximately half the image pixel size (the amplitude of the frequency encoding gradient here corresponds to an image pixel size of about 500 μm). Using the two-step phase cycle suppresses the SQC pathways (+1, −1) and (−1, −1) as shown in (F), with the four-step phase cycle offering additional suppression of the iZQC pathway (0, −1), as shown in (G). Data at a correlation distance of 260 μm were incomplete, and consequently this measurement is set to zero in the above contour plots, creating the discontinuity shown.

pathway (+1,−1) is refocused within the acquisition window of the imaging sequence when the correlation distance becomes larger than approximately half the in-plane pixel resolution. As shown previously [13,21] these additional coherence echoes can be significantly suppressed when using the two-step or four-step phase cycling schemes, as shown in Figs. 10F and G.

In practice, refocusing of the SQC pathway by the spatially encoding gradients should not be significant, since the proposed application is to probe the sample structure on a length scale that is significantly smaller than the image pixel dimensions. Although the refocusing of other coherence pathways also occurs when the correlation gradient is oriented in the phase encode direction, the interference may be avoided by aligning the correlation gradient parallel to the direction of the slice selecting gradient.

5. Conclusions

This work has demonstrated that residual SQCs arising from three different mechanisms can give rise to significant changes in unlocalized signal and image contrast in iMQC studies. These changes are similar to previously reported observations which have been attributed to the novel properties of iMQCs alone. Each of these SQC pitfalls can be avoided with appropriate precautions. An appropriate phase cycling scheme should be employed to suppress high spatial frequency components arising from undesired coherence pathways. Gradient cycling may be used to suppress stimulated echoes when investigating a range of correlation distances, without the need for long repetition times. In imaging experiments, when orienting the correlation gradient parallel to the direction of the frequency or phase encoding gradients, the correlation distance must be significantly smaller than the image pixel dimension in the orientation of the correlation gradient to avoid refocusing other coherence pathway echoes in the image k-space data, although again these can be suppressed via appropriate phase cycling.

In summary, it is important when attempting to characterize the novel iMQC contrast mechanism to ensure that residual SQCs are sufficiently suppressed, and that any observed changes in signal can be verified to arise from iMQCs alone. The potential applications of a sensitivity to sample structure at a specific user-definable length scale are significant. However, this mechanism has yet to be fully validated and understood. In particular, more work is required to demonstrate the suggested specific sensitivity of iMQCs to variations in the local magnetic field on a particular length scale, such as those arising from magnetic susceptibility mismatches between blood vessels and the surrounding tissue.

Acknowledgments

G.C-E. acknowledges useful conversations with Richard Bowtell and Warren Warren during the course of this work. This project was funded by Cancer Research UK [CRC] (C1060/A808/G7643) and the Medical Research Council [MRC].

References

[1] W.S. Warren, W. Richter, A.H. Andreotti, B.T. Farmer, Generation of impossible cross-peaks between bulk water and biomolecules in solution NMR, Science 262 (5142) (1993) 2005–2009.
[2] W. Richter, M. Richter, W.S. Warren, H. Merkle, P. Andersen, G. Adriany, K. Ugurbil, Functional magnetic resonance imaging with intermolecular multiple-quantum coherences, Magnetic Resonance Imaging 18 (5) (2000) 489–494.
[3] J.H. Zhong, E. Kwok, Z. Chen, FMRI of auditory stimulation with intermolecular double-quantum coherences (iDQCs) at 1.5 T, Magnetic Resonance in Medicine 45 (3) (2001) 356–364.
[4] G.D. Charles-Edwards, G.S. Payne, M.O. Leach, A. Bifone, Intermolecular double-quantum coherence imaging of brain tumours at 1.5 T, in: Proceedings of the Ninth International Meeting of the International Society of Magnetic Resonance in Medicine, Glasgow, 2001, p. 922.
[5] S. Capuani, G. Hagberg, F. Fasano, I. Indovina, A. Castriota-Scanderbeg, B. Maraviglia, In vivo multiple spin echoes imaging of trabecular bone on a clinical 1.5 T MR scanner, Magnetic Resonance Imaging 20 (2002) 623–629.
[6] S. Capuani, M. Alesiani, F.M. Alessandri, B. Maraviglia, Characterization of porous media structure by non linear NMR methods, Magnetic Resonance Imaging 19 (3–4) (2001) 319–323 (there is an error in the calculation of the correlation distance in this reference, which is too large by a factor of 2π).
[7] P. Robyr, R. Bowtell, Nuclear magnetic resonance microscopy in liquids using the dipolar field, Journal of Chemical Physics 106 (2) (1997) 467–476.
[8] R. Bowtell, P. Robyr, Structural investigations with the dipolar demagnetizing field in solution NMR, Physical Review Letters 76 (26) (1996) 4971–4974.
[9] S. Capuani, F. Curzi, F.M. Alessandri, B. Maraviglia, A. Bifone, Characterization of trabecular bone by dipolar demagnetizing field MRI, Magnetic Resonance in Medicine 46 (2001) 683–689 (there is an error in the calculation of the correlation distance in this reference, which is too large by a factor of 2π).
[10] F.M. Alessandri, S. Capuani, B. Maraviglia, Multiple spin echoes in heterogeneous systems: physical origins of the observed dips, Journal of Magnetic Resonance 156 (2002) 72–78 (there is an error in the calculation of the correlation distance in this reference, which is too large by a factor of 2π).
[11] R. Bowtell, S. Gutteridge, C. Ramanathan, Imaging the long-range dipolar field in structured liquid state samples, Journal of Magnetic Resonance 150 (2001) 147–155.
[12] L. Bouchard, R. Rizi, W.S. Warren, Physical origins of contrast in intermolecular multiple-quantum coherence imaging, in: Proceedings of the Ninth International Meeting of the International Society of Magnetic Resonance in Medicine, Glasgow, 2001, p. 526.
[13] L. Bouchard, R. Rizi, W.S. Warren, Magnetization structure based upon intermolecular multiple-quantum coherences, Magnetic Resonance in Medicine 48 (2002) 973–979.
[14] L. Bouchard, X. Tang, C. Chin, W.S. Warren, F.W. Wehrli, Structural characterization of trabecular bone using bulk NMR measurements of intermolecular multiple-quantum coherences, in:

Proceedings of the 11th International Meeting of the International Society of Magnetic Resonance in Medicine, Toronto, 2003, p. 1113.
[15] S. Gutteridge, C. Ramanathan, R.W. Bowtell, Microscopic susceptibility contrast in the crazed experiment, in: Proceedings of the 10th International Meeting of the International Society of Magnetic Resonance in Medicine, Honolulu, 2002, p. 615.
[16] S. Gutteridge, Imaging using long range dipolar field effects, Ph.D. thesis, University of Nottingham, 2002.
[17] J.P. Marques, R. Bowtell, Numerical simulations of the DQC signal in inhomogeneous solutions, in: Proceedings of the 11th International Meeting of the International Society of Magnetic Resonance in Medicine, Toronto, 2003, p. 1108.
[18] G. Deville, M. Bernier, J.M. Delrieux, NMR multiple echoes observed in solid 3He, Physical Review B 19 (11) (1979) 5666–5688.
[19] S. Lee, W. Richter, S. Vathyam, W.S. Warren, Quantum treatment of the effects of dipole–dipole interactions in liquid nuclear magnetic resonance, Journal of Chemical Physics 105 (3) (1996) 874–900.
[20] W. Richter, W.S. Warren, Intermolecular multiple quantum coherences in liquids, Concepts in Magnetic Resonance 12 (6) (2000) 396–409.
[21] E.D. Minot, P.T. Callaghan, N. Kaplan, Multiple echoes, multiple-quantum coherence, and the dipolar field: demonstrating the significance of higher order terms in the equilibrium density matrix, Journal of Magnetic Resonance 140 (1999) 200–205 (Eq. (9) in this reference contains a small error—$\sin^2\theta$ should read $\sin\theta$).
[22] J. Jeener, Equivalence between the "classical" and the "Warren" approaches for the effects of long range dipolar couplings in liquid nuclear magnetic resonance, Journal of Chemical Physics 112 (11) (2000) 5091–5094.
[23] The description of a demagnetizing time is sometimes felt to be inappropriate and the term dipolar angular velocity, $\omega_d \equiv 1/\tau_d$, may be used instead, e.g., J. Jeener, Collective effects in liquid NMR: dipolar field and radiation damping, in: D.M. Grant, R.K. Harris (Eds.), Encyclopaedia of Magnetic Resonance, Wiley, New York, 2002, pp. 642–679.
[24] Eq. (1) can be simplified for the case where $\beta = 90°$, (i.e., $\cos\beta = 0$), via the property $J_{n+1}(x) + J_{n-1}(x) = (2n/x)J_n(x)$. However, this compressed form hides the potential increase in the detected signal magnitude and the earlier onset of the signal peak that can be achieved by varying the second RF pulse angle.
[25] J.H. Zhong, Z. Chen, E. Kwok, In vivo intermolecular double-quantum imaging on a clinical 1.5 T MR scanner, Magnetic Resonance in Medicine 43 (3) (2000) 335–341 (the retainment of a single second order Bessel function in Eq. (3) of this reference to describe the complex transverse magnetization following an optimal second RF pulse angle of $\beta = 120°$ or 60° is not strictly correct. As noted above [25] when $\beta \neq 90°$ the simplification to a single second order Bessel function is no longer valid and the sum of the first and third order Bessel functions should be used).
[26] E.O. Stejskal, J.E. Tanner, Spin diffusion measurements: spin echoes in the presence of a time-dependent field gradient, Journal of Chemical Physics 42 (1965) 288.
[27] W.S. Warren, S. Ahn, M. Mescher, M. Garwood, K. Ugurbil, W. Richter, R.R. Rizi, J. Hopkins, J.S. Leigh, MR imaging contrast enhancement based on intermolecular zero quantum coherences, Science 281 (5374) (1998) 247–251.